JACS
JOURNAL OF THE AMERICAN CHEMICAL SOCIETY
Article
pubs.acs.org/JACS

Selectivity and Mechanisms Driven by Reaction Dynamics: The Case of the Gas-Phase OH^- + CH_3ONO_2 Reaction

Miguel A. F. de Souza,[†] Thiago C. Correra,[‡] José M. Riveros,*[,‡,§] and Ricardo L. Longo*[,†]

[†]Departamento de Química Fundamental, Universidade Federal de Pernambuco, 50.740-560 Recife, PE, Brazil
[‡]Instituto de Química, Universidade de São Paulo, Caixa Postal 26077, 05599-970 São Paulo, SP, Brazil
[§]Centro de Ciências Naturais e Humanas, Universidade Federal do ABC, Rua Santa Adelia 166, 09210-170 Santo André, SP, Brazil

Web-Enhanced Feature *Supporting Information*

ABSTRACT: Well-established statistical approaches such as transition-state theory based on high-level calculated potential energy profiles are unable to account for the selectivity observed in the gas-phase OH^- + CH_3ONO_2 reaction. This reaction can undergo bimolecular nucleophilic displacement at either the carbon center (S_N2@C) or the nitrogen center (S_N2@N) as well as a proton abstraction followed by dissociation ($E_{CO}2$) pathway. Direct dynamics simulations yield an S_N2:$E_{CO}2$ product ratio in close agreement with experiment and show that the lack of reactivity at the nitrogen atom is due to the highly negative electrostatic potential generated by the oxygen atoms in the ONO_2 group that scatters the incoming OH^-. In addition to these dynamical effects, the nonstatistical behavior of these reactions is attributed to the absence of equilibrated reactant complexes and to the large number of recrossings, which might be present in several ion−molecule gas-phase reactions.

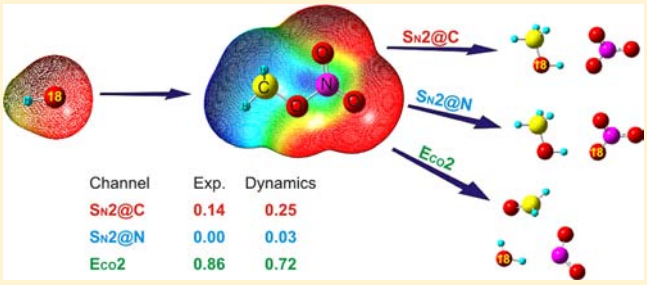

INTRODUCTION

The outcome and selectivity of chemical reactions are usually viewed within the context of statistical models such as transition-state theory (TST). For example, the kinetic selectivity between two reaction pathways starting from the same reactants is predicted to favor the product(s) formed through the smallest energy barrier. Under these conditions, the product ratio is expected to be determined by the difference in Gibbs activation energies. Accordingly, the reaction energy profiles (intrinsic reaction coordinate (IRC) pathways) and the assumption of a statistical distribution of microstates are sufficient to explain the behavior of a large number of reactions. However, in some cases the energy profile, or the IRC, does not uniquely determine the reaction outcome,[1−5] and examples of nonstatistical behavior[6] have been shown for a few gas-phase S_N2 reactions.[1,7−10] For these cases, Hase and co-workers have provided a detailed and comprehensive discussion of the importance of studying the dynamics of these reactions through trajectory calculations to probe mechanisms at the microscopic level.[11]

A recent study of the gas-phase reaction between OH^- and methyl nitrate (CH_3ONO_2) under high-vacuum conditions has posed some puzzling questions.[12] Three channels were calculated to be energetically possible, as shown in Scheme 1.

The experiments revealed the fast formation of NO_2^- and NO_3^- in a 0.86:0.14 ratio, but no displacement through the S_N2@N mechanism could be observed at near-thermal energies. The fact that no reaction occurs (within experimental error) by attack at the nitrogen center (S_N2@N) is surprising

Scheme 1. Reaction Pathways for the Isotopically Labeled OH^- Nucleophile and Methyl Nitrate

$$^{18}OH^- + CH_3ONO_2 \rightarrow \begin{cases} CH_3{}^{18}OH + ONO_2^- & S_N2@C \quad (1) \\ CH_3OH + {}^{18}ONO_2^- & S_N2@N \quad (2) \\ CH_2O + H_2{}^{18}O + NO_2^- & E_{CO}2 \quad (3) \end{cases}$$

because *ab initio* quantum chemical calculations at different levels suggest this pathway to be a barrierless process.[12] Understanding the reasons as to why the gas-phase OH^-/CH_3ONO_2 system avoids a feasible low-energy pathway is an intriguing problem that can provide considerable information on elementary reactions that can proceed through different mechanisms. Furthermore, these model gas-phase reactions of methyl nitrate are particularly relevant because light alkyl nitrates, as well as NO_3^- species, are known to play an important role in atmospheric chemistry[13,14] and to act as odd nitrogen reservoirs in the troposphere.[15−17] Thus, a thorough characterization of the reactive behavior of these substrates is of considerable interest.

In order to address the reactivity of methyl and related alkyl nitrates, we initially decided to carry out a reinvestigation of the energy surface for reactions (1)−(3) at higher levels of theory. While these calculations provide a more elaborate description of the reaction pathways, and particularly for the S_N2@N

Received: June 12, 2012
Published: October 29, 2012

   dx.doi.org/10.1021/ja3057166 | J. Am. Chem. Soc. 2012, 134, 19004−19010

channel, these new energy profiles are still unable to account for the selectivity of the different channels. We then decided to investigate these reactions by direct dynamics to explore whether dynamical features can account for the observed reactivity.

The direct dynamics approach reveals an unusual chemical system where the dynamics effectively controls the selectivity of non-bifurcating reaction channels[18,19] and explains the lack of reactivity at the N center. Furthermore, it provides some new insight on whether elimination-type reactions like reaction (3) proceed through a concerted or stepwise mechanism.

COMPUTATIONAL DETAILS

All electronic structure and Born−Oppenheimer molecular dynamics (BOMD) simulation calculations were performed with the Gaussian 09 program[20] using its default criteria. *Ab initio* HF, MP2, and CCSD(T)[21] as well as density functionals B3LYP[21] and M06-2X[22] were employed with 6-31+G(d) and 6-311+G(3df,2p) basis sets:[21] HF/6-31+G(d), B3LYP/6-31+G(d), M06-2X/6-31+G(d), MP2/6-31+G(d), MP2/6-311+G(3df,2p), and CCSD(T)/6-311+G(3df,2p)//MP2/6-311+G(3df,2p). These methods were selected mainly because MP2 and CCSD(T) are references for ion−molecule reactions in the gas phase that involve competing nucleophilic displacement and elimination pathways.[23−27] However, detailed studies of the dynamics are hindered by the high computational demand of MP2 and CCSD(T) calculations, so less demanding methods such as HF/6-31+G(d), B3LYP/6-31+G(d), M06-2X/6-31+G(d), and MP2/6-31+G(d) were also tested. All methods were validated by comparing the structures of the stationary points on the potential energy surface (PES) as well as their relative energies with respect to the CCSD(T)/CBS//MP2/6-311+G(3df,2p) reference method. The extrapolation to the complete basis set (CBS) limit was performed from CCSD(T)/aug-cc-pVXZ (X = D, T, and Q) calculations[28,29] with the ACESIII program.[30] The main goal of this validation procedure was to select a less demanding method to perform the BOMD simulations where thousands or even tens of thousands energy, gradient, and Hessian calculations are necessary to integrate a trajectory. The main stationary points on the PES of the OH^- + CH_3ONO_2 reaction were properly characterized by their Hessian, and the transition states were shown to connect a reactant to a product by the IRC approach.[31] It should be noticed that the IRC corresponds to the minimum energy path on the PES that connects the reactant to the product through the transition state.

RRKM calculations[32] were carried out for energy values from E^* = 21.0 to 74.6 kcal mol^{-1} using an in-house program.[33] The initial value of E was taken as the complexation energy of RC1 (E_{RC1}), the lowest energy content of the activated complexes under high-vacuum conditions. To calculate the RRKM rate constants consistent with the experimental conditions, the rate constants $k_a(E^*)$ were weighted by a Boltzmann distribution and integrated from E^* = 21.0 to 74.6 kcal mol^{-1} to yield the rate constants k_a. The MP2/aug-cc-pVTZ energies, structures, and vibrational frequencies used in the RRKM calculations are provided in the Supporting Information (Table S5).

The BOMD simulations were employed for the reactive and nonreactive scattering of OH^- on the CH_3ONO_2 substrate at several collision energies and relative orientations. The trajectories started at the reactant structures of the OH^- + CH_3ONO_2 system, and a quasi-classical sampling[34] was used. This sampling included the zero-point energy (ZPE) of each vibrational mode of the OH^- and CH_3ONO_2 fragments with random phases. In addition, rotational sampling was performed considering a Boltzmann distribution at 300 K of symmetric tops. An initial translational energy (E_{coll}) of 1.0 or 10.0 kcal mol^{-1} was given to the OH^- nucleophile or distributed randomly among the reactants. The value of 1.0 kcal mol^{-1} is compatible with a thermal energy of 300 K, and the higher translational energy was used to investigate the presence of reaction channels, particularly the S_N2@N pathway.

Monte Carlo approaches are usually recommended for determining rate constants because they can provide error estimates and moderate accuracy from a limited number of trajectories.[35,36] However, the rate constants were not measured experimentally, so our main goal is to explain the observed selectivity. We used the systematic approach depicted in Figure 1. This approach has been used to explore the S_N2/E2 selectivity in the F^- + C_2H_5Cl reaction[37] and can increase the relative number of reactive trajectories because these pathways have small impact parameters.[37] In addition, it can provide relationships between the reaction pathways and the relative orientations of the reactants. The geometric parameters (see Figure 1) used for the initial conditions of the trajectory simulations consisted of an initial distance (d) between the fragments (O atom at OH^- and CH_3ONO_2 center-of-mass) of 8.0 Å. The nucleophile was oriented around the CH_3ONO_2 substrate in five planes, namely, the plane xz corresponding to the C_s-symmetry plane, two perpendicular planes yz and xy, and two bisecting planes at 45° and 135°. For a collision energy (E_{coll}) of 1.0 kcal mol^{-1}, given either to the OH^- fragment or randomly assigned to both reactants, a total of 130 trajectories were generated by varying uniformly θ_{xz} and θ_{yz} in increments of 10° and θ_{xy}, θ_{45}, and θ_{135} in 15° increments. For E_{coll} = 10.0 kcal mol^{-1} assigned to the nucleophile, larger increments (20°) were used only for θ_{xz} and θ_{yz}, resulting in 36 trajectories. These trajectories were calculated at the M06-2X/6-31+G(d) level. Several other trajectories with different electronic structure methods and fragment orientations were calculated for comparison purposes.

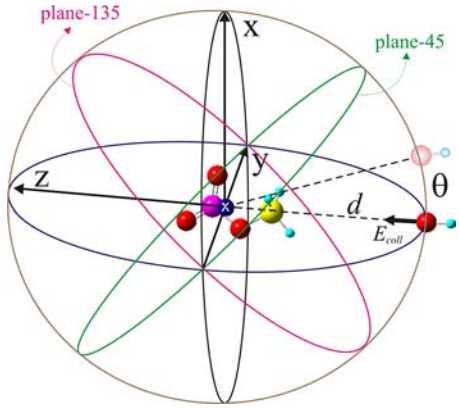

Figure 1. Coordinate frame and geometry of the CH_3ONO_2 + OH^- reacting system used in the initial conditions for BOMD simulations. The origin of the coordinate system is placed at the center-of-mass (X) of the methyl nitrate substrate, and its symmetry plane (C_s point) labels the plane xz. The OH^- is placed at a distance d from the origin in the planes xz, yz, xy, 45°, and 135° illustrated by the circles. E_{coll} represents the value of the translation energy, and the vector indicates its relative velocity. The angular orientation of the nucleophile is indicated by θ.

All BOMD simulations employed a Hessian-based predictor−corrector algorithm[38,39] with the prediction step performed in the normal coordinates, which does not conserve angular momentum.[39] However, the maximum deviations of the angular moment for all simulations were smaller than $10^{-6}\hbar$. In addition to being small, these deviations are insignificant because we are not interested in state-to-state analysis of the products, so the lack of angular momentum conservation should not affect our conclusions. All trajectories were integrated up to 2 ps or until the separation of the products exceeded 10 Å. The Hessian was computed at each propagation step.

RESULTS AND DISCUSSION

A more detailed analysis of the free-energy profiles for reactions (1)−(3) calculated at the CCSD(T)//MP2 level is shown in Figure 2. As for most exothermic gas-phase ion−molecule

dx.doi.org/10.1021/ja3057166 | J. Am. Chem. Soc. 2012, 134, 19004−19010

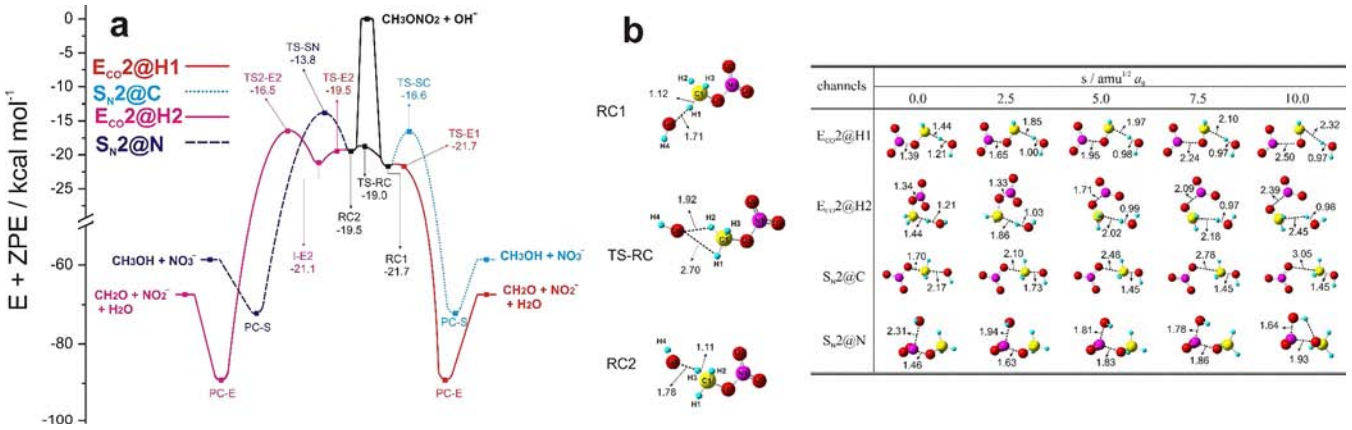

Figure 2. Energy profiles and structures for the OH^- + CH_3ONO_2 reaction. (a) Energy profiles (in kcal mol^{-1}) with inclusion of zero-point corrections (ZPE) calculated at the CCSD(T)/CBS//MP2/6-311+G(3df,2p) level. The relative energies are shown for the main stationary points and the reactant complex structures. (b) Calculated structures (distances in Å) at the MP2/6-311+G(3df,2p) level along selected values (s = 0.0 transition state, 2.5, 5.0, 7.5, and 10.0 amu$^{1/2}$ a_0) of the IRC after the transition state and along their respective pathway.

reactions, the initial ion-neutral reaction complexes and the transition states are lower in energy than the reactants.

Based on Figure 2, it should be pointed out that the S_N2@C and $E_{CO}2$@H1 pathways start at the reactant complex RC1, whereas the S_N2@N and $E_{CO}2$@H2 pathways are related to RC2. Notice a low-energy pathway that interconverts RC1 into RC2. The S_N2@C pathway is described by the typical double-well model,[1,7] while the S_N2@N involves an intermediate structure after the first transition state that disappears upon inclusion of the ZPE corrections and entropic contributions. These calculated profiles reveal two distinct elimination pathways. Abstraction of the proton in the symmetry plane of the CH_3ONO_2 substrate starts with the reactant complex RC1 and follows a pathway ($E_{CO}2$@H1) different from that associated with RC2 ($E_{CO}2$@H2), which removes either of the equivalent protons off the symmetry plane. The details of these pathways after the transition state are presented in Figure 2b. The proton abstraction and the O_2N-OCH_3 bond dissociation are concerted steps in the $E_{CO}2$@H1 pathway, but they are asynchronous for the $E_{CO}2$@H2 mechanism because the $-NO_2$ group needs to perform an internal rotation to induce the N−O bond cleavage. These two pathways ($E_{CO}2$@H1 and $E_{CO}2$@H2 or E1cb-like) are limiting cases in a spectrum of continuous reaction mechanisms ranging from synchronous to non-synchronous eliminations.[40]

In order to account for the product distribution reported in ref 12, an initial attempt was made to estimate the branching ratios that would be expected on the basis of RRKM calculations starting from the RC1 and RC2 complexes. The first important result from these calculations is that the rate constants for the elimination channels are estimated to be orders of magnitude more favorable than the substitution channels, based on MP2/aug-cc-pVTZ calculations (see Table S5). For example, RRKM calculations starting from the RC1 complex predict that 100% of the reaction would proceed through the $E_{CO}2$@H1 mechanism. A more complete kinetic scheme, as shown in Scheme 2, allowing for the interconversion of RC1 and RC2, yields similar results, with both RC1 and RC2 favoring the elimination pathways exclusively (see Figure S4 and Table S6).

RRKM calculations were also carried out at the CCSD(T)/CBS//MP2/6-311+G(3df,2p) level of theory and yield results

Scheme 2. Kinetic Scheme for the Various Unimolecular Reaction Pathways Originating from the RC1 and RC2 Reactant Complexes Shown in Figure 2

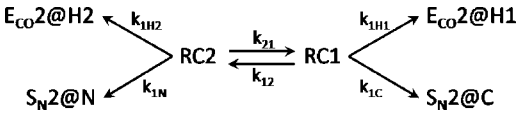

similar to those obtained with the MP2/aug-cc-pVTZ method, as shown in Figure S4b and Table S6.

The main difference between these results is the increase in the S_N2@C rate when compared to the S_N2@N pathway and the inversion in the H1 and H2 elimination rate constants values. All these changes can be rationalized by the subtle decrease in the H2 and C reaction barriers and the increased barrier calculated for the N and H1 routes at the CCSD(T)/CBS level of theory.

The kinetic model used above reveals the inability of a purely statistical approach to account even for the fact that the S_N2@C mechanism is competitive with the $E_{CO}2$ mechanism as observed experimentally, regardless of the level of theory used. Thus, it is questionable whether this approach can explain the lack of reactivity through the S_N2@N mechanism. We therefore proceeded to investigate this system by BOMD simulations.[34]

Because of the high computational cost of these simulations, less demanding *ab initio* (HF and MP2) and density functional theory (DFT) methods (B3LYP, M06-2X) were tested. The M06-2X/6-31+G(d) method proved to yield the best overall performance for relative energies, shape of the IRCs and structures for all four reaction pathways (see Figures S1−S3 in Supporting Information). Thus, 130 and 36 trajectories were calculated with this method for translational energies of 1.0 and 10.0 kcal mol^{-1}. All trajectories were integrated up to 2 ps or until the separation of the fragments exceeded 10 Å and quasi-classical samplings[34] of the vibrational modes were employed.

A quantitative analysis of the trajectories depicted in Figure 3 for scatterings in the planes *xz* and *yz* (see Schemes S1 and S2 and Tables S7 and S8 in Supporting Information) showed 78.9% of the collisions to be reactive, which leads to a good predicted reaction efficiency and significant statistics for the calculated selectivity. Our calculated S_N2:E2 product ratio of 0.29:0.71 is in reasonable agreement with the experimental

dx.doi.org/10.1021/ja3057166 | J. Am. Chem. Soc. 2012, 134, 19004−19010

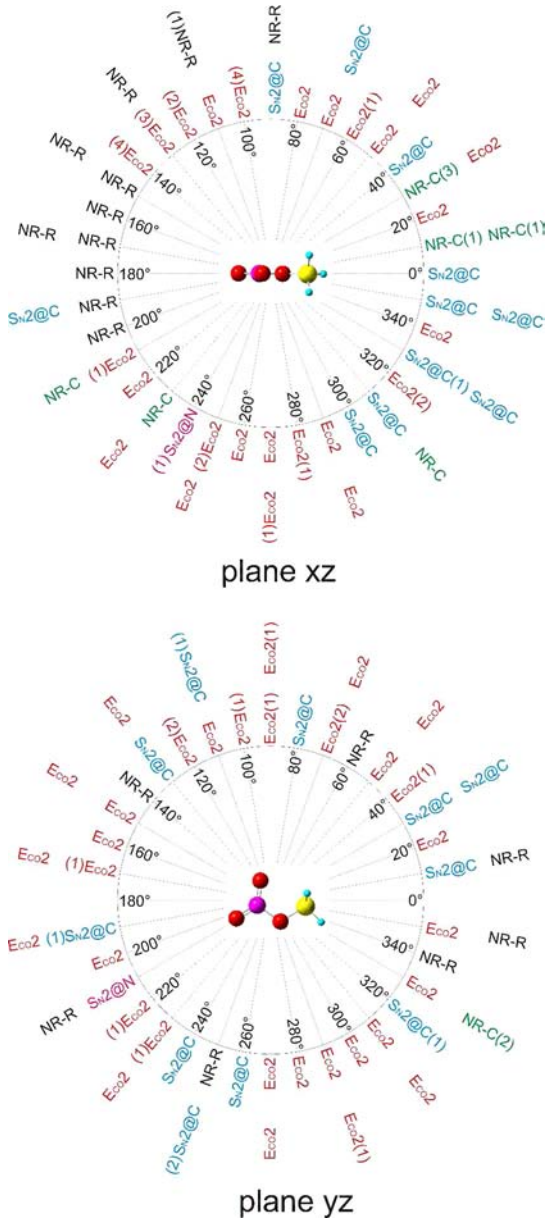

Figure 3. Trajectories for the OH^- + CH_3ONO_2 reaction. Classification of the trajectories according the initial conditions: angle (degrees), collision plane (xz is the molecular symmetry plane), and collision energy (1.0 kcal mol^{-1} is the inner sphere, and 10.0 kcal mol^{-1} is the outer sphere) obtained with the M06−2X/6-31+G(d) method (see Computational Details). Notation: NR-R and NR-C are unreactive collisions that backscatter to the reactants and remain as a complex for 2 ps, S_N2@C and S_N2@N are nucleophilic displacements at the carbon and nitrogen centers, and $E_{CO}2$ are eliminations. The numbers in parentheses are the number of recrossings during the trajectory.

data[12] and the calculated ratios are almost independent of the collision energy. The contribution of the S_N2@N pathway is smaller than 4%, which is comparable with the original experimental detection limit. Considering only the trajectories in the planes *xz* and *yz* with the collision energies 1.0 and 10.0 kcal mol^{-1} given to the OH^- fragment, amounting to 70 and 36 trajectories (see Figure 3), respectively, a S_N2:E2 product ratio of 0.28:0.72 (see Table S8 in Supporting Information) is obtained. This result suggests that the calculated S_N2:E2 selectivity is converged with respect to the initial conditions and that the errors are ca. 3% estimated from the standard deviation of a binomial distribution (reactive or nonreactive trajectory). This error is close to that estimated for the dynamics study of the F^- + CH_3OOH reaction with a similar number of trajectories chosen randomly.[36]

The dynamical approach can also provide details of the atomic motions (see Movies S1−S5 in Supporting Information), and some representative trajectories are depicted in Figure 4.

Figure 4-ii and iii illustrates selected $E_{CO}2$@H1 and $E_{CO}2$@H2 pathways that emphasize the synchronicity and concertedness aspects of these mechanisms.[41,42] The $E_{CO}2$@H1 pathway is faster than the $E_{CO}2$@H2 because the latter pathway requires an internal rotation (motion between 1150 and 1450 fs in Figure 4-iii) of the $-NO_2$ group for a proper alignment of the electron densities to induce the dissociation. The $E_{CO}2$@H1 pathway is concerted and practically synchronous because the proton transfer occurs at ca. 700 fs and the N−O bond dissociation occurs within a few vibrational periods at ca. 770 fs. The $E_{CO}2$@H2 mechanism has a distinct dynamical behavior with the proton transfer occurring at ca. 1150 fs, significantly earlier than the N−O bond dissociation at ca. 1600 fs, thus being an asynchronous process. Furthermore, the $[CH_2ONO_2]^-$ intermediate has a lifetime long enough to undergo internal rotation and several vibrational periods, so this pathway might also be considered nonconcerted, or otherwise an E1cb-like mechanism.[40] A quantitative analysis (see Figure S6 in Supporting Information) of the elapsed time between these two events, i.e., proton abstraction (H···O forming bond ≤1 Å) and dissociation of the N−O bond (≥2 Å), showed that the elimination reactions involve an almost continuous spectrum of mechanisms ranging from synchronous to highly asynchronous and possibly nonconcerted pathways.

Figure 4-iv illustrates one of the two trajectories (calculated at the M06-2X level) that resulted in the S_N2@N product. This trajectory involves rotation of the CH_3ONO_2 molecule to maximize the attraction between the incoming OH^- and the CH_3 group. Conservation of angular momentum leads to a geometry that resembles the RC2 structure (see Figure 2b) at ca. 610 fs followed by a structure similar to the transition state (see Figure 2b) at ca. 700 fs, ensued by an internal rotation of the OH^- moiety during the next ca. 100 fs to dissociate into the products.

Figure 4-i depicts a typical S_N2@C trajectory and shows the distorted trigonal bipyramid (Figure 4-i, 970 fs) transition state structure usually associated with the S_N2 mechanism.[1,43] In addition, Figure 4-i illustrates an interesting trajectory where an initial proton abstraction by the nucleophile allows for energy transfer from the nucleophile to the substrate and activation of the S_N2@C pathway. In the meantime, one of the S_N2@C trajectories at 10.0 kcal mol^{-1} of collision energy involved the indirect roundabout mechanism (see Movie S5 in Supporting Information) observed for collisions (at ca. 44 kcal mol^{-1}) of Cl^- with CH_3I where the neutral species performs a complete rotation before the nucleophilic displacement.[43] Notice, however, that for the OH^- + CH_3ONO_2 reaction the non-hydrogen atoms (carbon, nitrogen and oxygen) have similar masses, whereas in the Cl^- + CH_3I reaction the masses of the nucleophile (Cl^-) and the leaving group (I^-) are very different and might facilitate the roundabout mechanism.

The S_N2@C/S_N2@N selectivity observed in the simulations can be attributed to the dynamic control exerted by the long-range electrostatic interactions.

dx.doi.org/10.1021/ja3057166 | J. Am. Chem. Soc. 2012, 134, 19004−19010

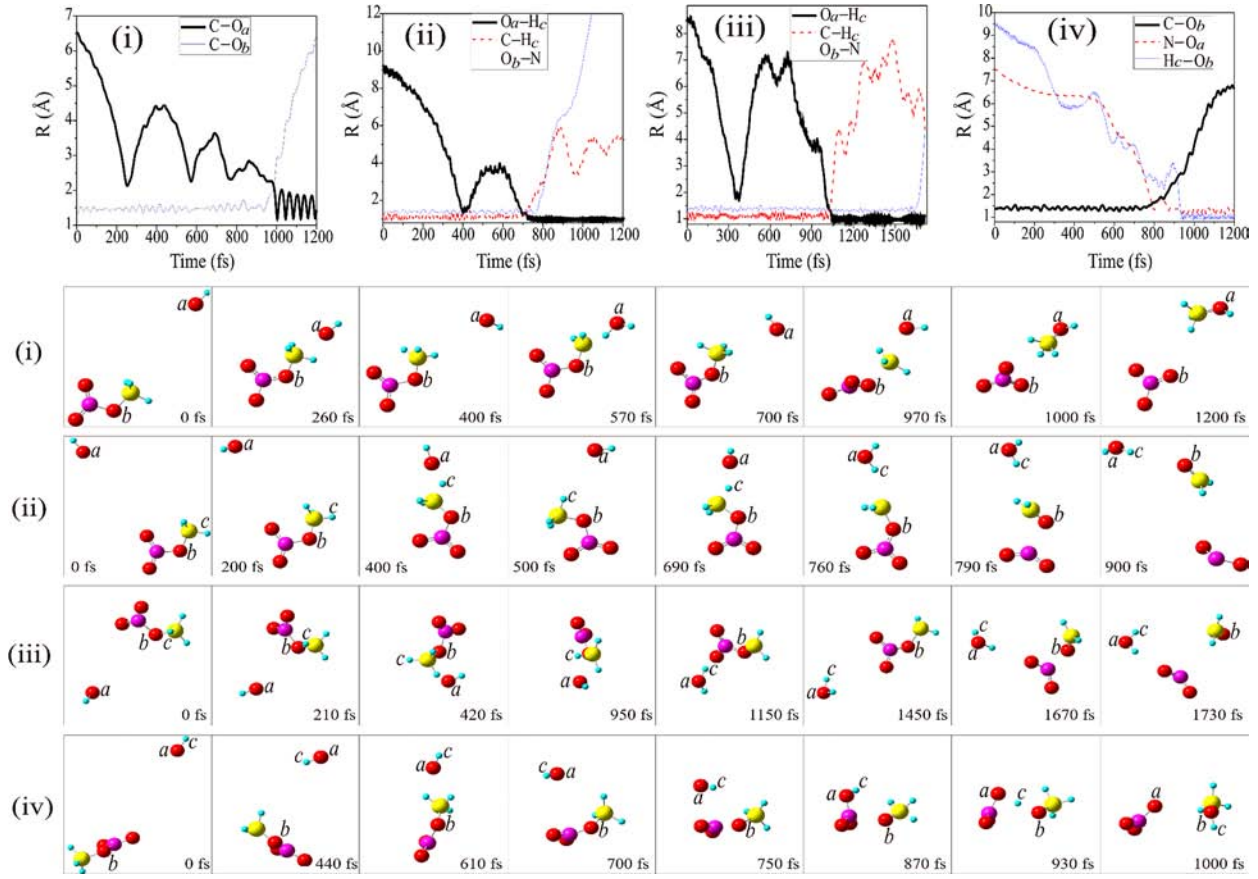

Figure 4. Representative trajectories dynamics for the OH^- + CH_3ONO_2 reaction. Top panel: relevant interatomic distances (in Å) for the (i) S_N2@C, (ii) $E_{CO}2$@H1, (iii) $E_{CO}2$@H2, and (iv) S_N2@N pathways. Lower panel: relevant structures along a (i) S_N2@C, (ii) $E_{CO}2$@H1, (iii) $E_{CO}2$@H2, and (iv) S_N2@N trajectories. The atomic labels are shown in the figures in the lower panel. Videos for each trajectory are available in the online version.

The dynamical behavior of the trajectories observed in the simulations and the corresponding calculated energy profile can be interpreted with the help of the electrostatic potentials of the methyl nitrate and hydroxyl illustrated in Figure 5.

It is noticeable that the electrostatic potential near the nitrogen center is highly positive, so the transition state would be predicted to be stabilized by the attractive interactions of the nucleophile near this center. On the other hand, the less positive electrostatic potential at the carbon atom could be expected to lead to a higher energy barrier for the S_N2@C pathway compared to S_N2@N, as schematically represented by the dashed arrows in Figure 5. However, the highly positive potential at the nitrogen is shielded by a very negative electrostatic potential from the oxygen atoms that can explain the lack of reactivity on the nitrogen observed in the dynamics. Namely, the nucleophile is scattered by the negative electrostatic potential generated by the oxygen atoms during the collisions of OH^- with CH_3ONO_2. Interestingly enough, all trajectories with the OH^- initially directed toward the nitrogen atom to promote the S_N2@N reaction were either deflected or induced a rotation of the neutral substrate to yield a reaction along the S_N2@C or $E_{CO}2$ pathways. These features are general in all BOMD simulations regardless of the electronic structure method.

A detailed analysis of Figure 3 shows that the $E_{CO}2$ trajectories are nearly independent of the relative orientation of the nucleophile with respect to the methyl nitrate substrate, whereas the S_N2@C trajectories are mostly restricted to near-frontal collisions on the methyl group, namely within ±60° around the C−O bond axis (Figure 3). These patterns were observed in these figures because the initial configurations were chosen systematically and they might be relevant for understanding the differences between the S_N2@C and $E_{CO}2$ pathways, and thus the reaction selectivity. The behavior of the S_N2@C mechanism was previously described for halogen exchange reactions (Cl^- + CH_3 X, with X = Cl and Br)[1] as well as for the OH^- + CH_3Cl → CH_3OH + Cl^- reaction[45] and agrees with a proposed dynamical model involving intermolecular and intramolecular complexes.[1,7,9] In this model, the reactants form an intermolecular complex that still has most of its collision energy in the translational degrees of freedom. The coupling between the translational degrees of freedom with the vibrational modes allows for this energy to be redistributed and to form an intramolecular complex that is equivalent to the reactant complexes RC1 or RC2 in Figure 2b. If the energy equilibration is accomplished then statistical models are applicable and should provide reasonable results. However, for the S_N2 reactions Cl^- + CH_3X (X = Cl, Br), the translational−vibrational energy redistribution is slow compared to the direct reaction rate and thus precludes the use of statistical theories.[1,7,9] Alternatively, the lifetimes of the intramolecular complexes are too short to be amenable to a statistical modeling. In fact, measurements for several S_N2 reactions of halide ions with monohalogenated methanes such as F^- + CH_3X (X = Cl, Br, I) cannot be described by statistical theories.[44] The observation that for slightly larger reactants the

dx.doi.org/10.1021/ja3057166 | J. Am. Chem. Soc. 2012, 134, 19004−19010

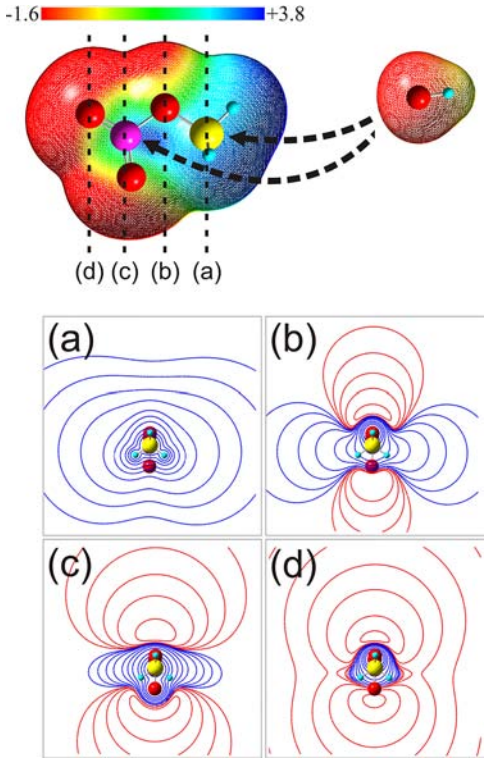

Figure 5. Top panel: electrostatic potentials of CH_3ONO_2 and OH^- calculated at the MP2/6-311+G(3df,2p) level. The dashed arrows represent the preferable S_N2 pathways. In the lower panel (a), (b), (c), and (d) are contour plots of the electrostatic potential on the planes passing through the carbon, oxygen (N−O−C), nitrogen, and oxygen (terminal) atoms perpendicular to the symmetry plane of the molecule.

kinetics of the S_N2 reaction $^{37}Cl^- + {}^{35}ClCH_2CN \rightarrow {}^{35}Cl^- + {}^{37}ClCH_2CN$ is properly described by the RRKM theory suggests that the nonstatistical behavior of halogen exchange reactions $X^- + CH_3Y$ at energies near the room temperature is not a general phenomenon.[9,44] Indeed, it was shown that the nearly thermoneutral reactions $^{37}Cl^- + m\text{-}FC_6H_4CH_2{}^{35}Cl \rightarrow {}^{35}Cl^- + m\text{-}FC_6H_4CH_2{}^{37}Cl$ and $^{37}Cl^- + RC_6H_4C(O){}^{35}Cl \rightarrow {}^{35}Cl^- + RC_6H_4C(O){}^{37}Cl$ (R = *m*-F, *m*-CF_3, H, *m*-CH_3, *p*-CH_3) involving large organic substrates also behave statistically.[9] These results thus suggest that the statistical or nonstatistical behavior may be related to the number of vibrational modes of the intermolecular complexes. However, S_N2 halogen exchange reactions of multihalogenated methanes $F^- + CF_3X$ (X = Cl, Br, I) also show statistical behavior,[44] which could be explained by the long lifetimes of the intramolecular complexes because of the observation of association channels. Thus, the fact that the reactivity pattern of the gas-phase $OH^- + CH_3ONO_2$ reaction cannot be adequately described by the usual statistical theories is quite relevant because the intermolecular complex has almost twice (27 versus 15) the vibrational modes of the $X^- + CH_3Y$ systems and shows that the dynamics may determine the outcome of several other S_N2 reactions.

Lastly, the qualitative agreement between the calculated and observed product ratio for the S_N2@C and $E_{CO}2$ channels is remarkable considering that (i) the M06-2X calculated barrier for the S_N2@C mechanism is slightly lower (ca. 0.8 kcal mol^{-1}) than the reference value (CCSD(T)//MP2), (ii) no tunneling effects were included in the simulations for the proton abstraction in the elimination channels, and (iii) the energy transfer from the translational motion of the nucleophile to the vibrational modes of the substrate is not quantized because of the classical treatment of the nuclear motions. This caveat overestimates the energy transfer among the nuclear motions and thus possibly the cross sections for S_N2 reactions.

CONCLUSION

The dynamics of the simple reactions in (1)−(3) have been shown to be extremely rich and provide us with some unusual insight on these reactions. For example, the lack of formation of reactant complexes with lifetimes long enough for energy equilibration suggests a nonstatistical behavior of the $OH^- + CH_3ONO_2$ reaction. As a matter of fact, 30% of the reactive trajectories yield the products in a single event and for all the remaining trajectories the products are formed within ca. 2 ps, which is well below the required time for energy redistribution and equilibration.[1,7,9] Interestingly enough, 30% of the reactive trajectories, mostly elimination, presented at least one recrossing (Figure 3). For instance, Figure 4-i illustrates recrossings between 400 and 700 fs where the proton is abstracted, water is formed and the system returns to regenerate the reactants. This behavior is not accounted for in the traditional TST and more elaborate statistical approaches would be required for a proper description of the selectivity.

Yet, the most dramatic conclusion of our work is to show how reaction selectivities and mechanisms are controlled by the dynamics and long-range electrostatic interactions of the $OH^- + CH_3ONO_2$ system.[46] This is the first case to our knowledge where the dynamics clearly reveal how a reaction avoids a feasible low energy pathway such as the nucleophilic displacement at nitrogen, and may determine the selectivity in related systems.

ASSOCIATED CONTENT

Supporting Information

Tables with relative energies, total energies, structures (including Cartesian coordinates), and vibrational frequencies for all optimized species; figures with additional results and analyses; movies S1−S5 showing trajectories. This material is available free of charge via the Internet at http://pubs.acs.org.

Web-Enhanced Feature

Four movies, in .avi format, showing the trajectories in Figure 4.

AUTHOR INFORMATION

Corresponding Author

longo@ufpe.br; jmrnigra@iq.usp.br

Notes

The authors declare no competing financial interest.

ACKNOWLEDGMENTS

The Brazilian Agencies CNPq, CAPES, FACEPE, FAPESP, and FINEP are acknowledged for providing financial support under grants Pronex APQ-0859-1.06/08 and INCT-INAMI Proc. no. 573986/2008-8 and INCT-INOMAT. M.A.F.S. and T.C.C. thank CNPq for graduate scholarships. Dr. Marcus V. P. dos Santos is acknowledged for helping with the CCSD(T) calculations performed at the CENAPAD-PE.

REFERENCES

(1) Hase, W. L. *Science* **1994**, *266*, 998−1002.
(2) Sun, L.; Song, K.; Hase, W. L. *Science* **2002**, *296*, 875−878.

(3) Ammal, S. C.; Yamataka, H.; Aida, M; Dupuis, M. *Science* **2003**, *299*, 1555−1557.
(4) Bekele, T.; Christian, C. F.; Lipton, M. A.; Singleton, D. A. *J. Am. Chem. Soc.* **2005**, *127*, 9216−9223.
(5) dos Santos, M. V. P.; Teixeira, E. S.; Longo, R. L. *J. Braz. Chem. Soc* **2009**, *20*, 652−662.
(6) Glowacki, D. R.; Harvey, J. N.; Mulholland, A. J. *Nature Chem.* **2012**, *4*, 169−176.
(7) Chabinyc, M. L.; Craig, S. L.; Regan, C. K.; Brauman, J. I. *Science* **1998**, *279*, 1882−1886.
(8) Vanorden, S. L.; Pope, R. M.; Buckner, S. W. *Org. Mass Spectrom.* **1991**, *26*, 1003−1007.
(9) Craig, S. L.; Zhong, M.; Brauman, J. I. *J. Am. Chem. Soc.* **1999**, *121*, 11790−11797.
(10) Tonner, D. S.; McMahon, T. B. *J. Am. Chem. Soc.* **2000**, *122*, 8783−8784.
(11) Manikandan, P.; Zhang, J.; Hase, W. L. *J. Phys. Chem. A* **2012**, *116*, 3061−3080.
(12) Correra, T. C.; Riveros, J. M. *J. Phys. Chem. A* **2010**, *114*, 11910−11919.
(13) (a) Roberts, J. M. *Atmos. Environ.* **1990**, *24A*, 243−287. (b) Atkinson, R.; Arey, J. *Chem. Rev.* **2003**, *103*, 4605−4638.
(14) For the role of NO_3^- species, see: (a) Beig, G.; Brasseur, G. P. *J. Geophys. Res., Atmos.* **2000**, *105*, 22671−22684. (b) Smith, D.; Spanel, P. *Mass Spectrom. Rev.* **1995**, *14*, 225−278.
(15) Chuck, A. L.; Turner, S. M.; Liss, P. S. *Science* **2002**, *297*, 1151−1154.
(16) Blake, N. J.; Blake, D. R.; Sive, B. C.; Katzenstein, A. S.; Meinardi, S.; Wingenter, O. W.; Atlas, E. L.; Flocke, F.; Ridley, B. A..; Rowland, F. S. *J. Geophys. Res.* **2003**, *108*, 8359−8374.
(17) He, S.; Chen, Z.; Zhang, X. *Environ. Res.* **2011**, *8*, 529−542 and references therein.
(18) Rehbein, J.; Carpenter, B. K. *Phys. Chem. Chem. Phys.* **2011**, *13*, 20906−20922.
(19) Hong, Y. J.; Tantillo, D. J. *Nature Chem.* **2009**, *1*, 384−389.
(20) Frisch, M. J.; Trucks, G. W.; Schlegel, H. B.; Scuseria, G. E.; Robb, M. A.; Cheeseman, J. R.; Scalmani, G.; Barone, V.; Mennucci, B.; Petersson, G. A.; Nakatsuji, H.; Caricato, M.; Li, X.; Hratchian, H. P.; Izmaylov, A. F.; Bloino, J.; Zheng, G.; Sonnenberg, J. L.; Hada, M.; Ehara, M.; Toyota, K.; Fukuda, R.; Hasegawa, J.; Ishida, M.; Nakajima, T.; Honda, Y.; Kitao, O.; Nakai, H.; Vreven, T.; Montgomery, J. A., Jr.; Peralta, J. E.; Ogliaro, F.; Bearpark, M.; Heyd, J. J.; Brothers, E.; Kudin, K. N.; Staroverov, V. N.; Kobayashi, R.; Normand, J.; Raghavachari, K.; Rendell, A.; Burant, J. C.; Iyengar, S. S.; Tomasi, J.; Cossi, M.; Rega, N.; Millam, J. M.; Klene, M.; Knox, J. E.; Cross, J. B.; Bakken, V.; Adamo, C.; Jaramillo, J.; Gomperts, R.; Stratmann, R. E.; Yazyev, O.; Austin, A. J.; Cammi, R.; Pomelli, C.; Ochterski, J. W.; Martin, R. L.; Morokuma, K.; Zakrzewski, V. G.; Voth, G. A.; Salvador, P.; Dannenberg, J. J.; Dapprich, S.; Daniels, A. D.; Farkas, Ö.; Foresman, J. B.; Ortiz, J. V.; Cioslowski, J.; Fox, D. J. *Gaussian 09*, Revision A.02; Gaussian, Inc.: Wallingford, CT, 2009.
(21) Cramer, C. J. *Essentials of Computational Chemistry—Theories and Models*, 2nd ed.; Wiley: New York, 2004.
(22) Zhao, Y.; Truhlar, D. G. *Theor. Chem. Acc.* **2008**, *120*, 215−241.
(23) Gronert, S. *J. Am. Chem. Soc.* **1991**, *113*, 6041−6048.
(24) Merrill, G. N.; Gronert, S.; Kass, S. R. *J. Phys. Chem. A* **1997**, *101*, 208−218.
(25) Bento, A. P.; Solà, M.; Bickelhaupt, F. M. *J. Chem. Theory Comput.* **2008**, *4*, 929−940.
(26) Pabis, A.; Paluch, P.; Szala, J.; Paneth, P. *J. Chem. Theory Comput.* **2009**, *5*, 33−36.
(27) Zhao, Y.; Truhlar, D. G. *J. Chem. Theory Comput.* **2010**, *6*, 1104−1108.
(28) Yao-Yuan Chuang, Y.-Y.; Truhlar, D. G. *J. Phys. Chem. A* **1999**, *103*, 651−652.
(29) Huh, S. B.; Lee, J. S. *J. Chem. Phys.* **2003**, *118*, 3035−3042.
(30) Lotrich, V.; Flocke, N.; Ponton, M.; Yau, A. D.; Perera, A.; Deumens, E.; Bartlett, R. J. *J. Chem. Phys.* **2008**, *128*, 194104−15.
(31) Fukui, K. *Acc. Chem. Res.* **1981**, *14*, 363−368.
(32) Robinson, P.; Holbrook, K. A. *Unimolecular Reactions*; John Wiley & Sons: New York, 1972.
(33) Pradie, N. A.; Linnert, H. V. *SuperRRKM*, version 1.0; University of São Paulo: São Paulo, Brazil, 2009.
(34) Sun, L.; Hase, W. L. *Rev. Comput. Chem.* **2003**, *19*, 79−146.
(35) Truhlar, D. G.; Muckerman, J. T. In *Atom−Molecule Collision Theory: a Guide for the Experimentalist*; Bernstein, R. B., Ed.; Plenum Press: New York, 1979; pp 505−566.
(36) López, J. G.; Vayner, G.; Lourderaj, U.; Addepalli, S. V.; Kato, S.; deJong, W. A.; Windus, T. L.; Hase, W. L. *J. Am. Chem. Soc.* **2007**, *129*, 9976−9985.
(37) Mugnai, M.; Cardini, G.; Schettino, V. *J. Phys. Chem. A* **2003**, *107*, 2540−2547.
(38) Millam, J. M.; Bakken, V.; Chen, W.; Hase, W. L.; Schlegel, H. B. *J. Chem. Phys.* **1999**, *111*, 3800−3805.
(39) Lourderaj, U.; Song, K.; Windus, T. L.; Zhuang, Y.; Hase, W. L. *J. Chem. Phys.* **2007**, *126*, 044105−11.
(40) Ensing, B.; Laio, A.; Gervasio, F. L.; Parrinello, M.; Klein, M. L. *J. Am. Chem. Soc.* **2004**, *126*, 9492−9493.
(41) Trost, B. M.; Miller, M. L. *J. Am. Chem. Soc.* **1988**, *110*, 3687−3689.
(42) Diau, E. W.-G.; De Feyter, S.; Zewail, A. H. *Chem. Phys. Lett.* **1999**, *304*, 134−144.
(43) Mikosch, J.; Trippel, S.; Eichhorn, C.; Otto, R.; Lourderaj, U.; Zhang, J. X.; Hase, W. L.; Weidemüller, M.; Wester, R. *Science* **2008**, *319*, 183−186.
(44) Morris, R. A.; Viggiano, A. A. *J. Phys. Chem.* **1994**, *98*, 3740−3746.
(45) Tachikawa, H.; Igarashi, M. *Chem. Phys.* **2006**, *324*, 639−646.
(46) For a recent example where dynamics are shown to control stereoselectivity, see: Glowacki, D. R.; Marsden, S. P.; Pilling, M. J. *J. Am. Chem. Soc.* **2009**, *131*, 13896−13897.